Yi et al. *Zool. Res.* 2025, 46(2): 446−458
https://doi.org/10.24272/j.issn.2095-8137.2024.391
https://cstr.cn/32248.14.zr.2024.391

ZR | Zoological Research

Article Open Access

Consistency, distinction, and potential metabolic crosstalk of nitrogen mobilization-related genes in silk production and silk gland biology

Mei-Yan Yi[1,#], Xu Yang[2,3,#], Man Wang[1], Jing-Wei Chen[1], Jia-Hao Xiang[1], Li-Jun Xiang[1], Lan-Sa Qian[2,3], Dong-Bin Chen[2,3], Yong-Ping Huang[4], Xiao-Ling Tong[5,*], Zu-Lian Liu[4,*], Hui Xiang[1,*]

[1] *Guangdong Provincial Key Laboratory of Insect Developmental Biology and Applied Technology*, *Institute of Insect Science and Technology*, *School of Life Sciences*, *South China Normal University*, *Guangzhou*, *Guangdong* 510631, *China*

[2] *Key Laboratory of Insect Developmental and Evolutionary Biology*, *Center for Excellence in Molecular Plant Sciences*, *Shanghai Institute of Plant Physiology and Ecology*, *Chinese Academy of Sciences*, *Shanghai* 200032, *China*

[3] *University of Chinese Academy of Sciences*, *Beijing* 100049, *China*

[4] *School of Environmental Science and Engineering*, *Shanghai Jiao Tong University*, *Shanghai* 200240, *China*

[5] *State Key Laboratory of Resource Insects*, *Key Laboratory for Sericulture Biology and Genetic Breeding*, *Ministry of Agriculture and Rural Affairs*, *College of Sericulture*, *Textile and Biomass Sciences*, *Southwest University*, *Chongqing* 400715, *China*

ABSTRACT

The domesticated silkworm (*Bombyx mori*) has evolved a highly efficient nitrogen utilization system to support silk production. The silk glands play a pleiotropic role in sequestering nitrogen resources for silk synthesis, mitigating aminoacidemia by assimilating free amino acids, and reallocating nitrogen during metamorphosis through programmed cell death. However, the specific functions of nitrogen metabolism-related genes in this process remain unclear. Using CRISPR/Cas9-based gene editing, mutations were generated in glutamine synthetase (*GS*), glutamate synthetase (*GOGAT*), asparagine synthetase (*AS*), glutamate dehydrogenase (*GDH*) and glutamate oxaloacetate transaminase 1 (*GOT1*). Disruption of *GS*, *GOGAT*, and *AS* consistently reduced silkworm cocoon and pupal weight and significantly down-regulated silk protein gene transcription, whereas *GOT1* mutation had no such effect. *GOGAT* mutants exhibited abnormally enlarged silk glands, whereas *GS* and *AS* mutants showed delayed programmed cell death in the silk glands. In contrast, *GOT1* mutants displayed normal silk gland morphology but were consistently smaller. Disruption of *GS*, *GOGAT*, and *AS* led to more extensive transcriptional changes, including altered expression of transcription factors in the silk glands, compared with *GOT1* mutants. Both *GS* and *GOGAT* mutants exhibited up-regulation of *AS* and *GDH*, while only *GOGAT* mutants displayed elevated AS enzymatic activity, suggesting that GOGAT may compete with AS for glutamine in the silk glands to support silk protein synthesis. *AS* mutants showed significantly elevated GOT activity and up-regulation of several metabolic pathways, indicating that AS may functionally interact with GOT in regulating both silk gland development and programmed cell death during metamorphosis.

Keywords: Silkworm; Nitrogen mobilization; Silk gland; Metamorphosis

INTRODUCTION

Silk production is a common adaptation among lepidopteran insects, with cocoon spinning serving a crucial ecological role in protecting pupae from microbial infections, predation, and environmental fluctuations. However, this process imposes a significant nitrogen demand (Daimon et al., 2010; Xia et al., 2009). Silk synthesis involves a highly coordinated system of nitrogen and amino acid metabolism, silk gland development, and the transcriptional and translational regulation of silk protein genes. The domesticated cocoon-producing silkworm (*Bombyx mori*) has garnered significant attention due to its exceptional silk-producing capacity. As *B. mori* larvae reach the final instar, the silk glands undergo rapid expansion, driven by active DNA replication, ribosome biogenesis, and high expression of silk protein genes (Xia et al., 2014).

Received: 07 November 2024; Accepted: 17 December 2024; Online: 18 December 2024

Foundation items: This work was supported by the National Natural Science Foundation of China (32270458, 32070411, 2023A1515010657) and State Key Laboratory of Resource Insects (SKLSGB-ORP202209)

[#]Authors contributed equally to this work

*Corresponding authors, E-mail: xltong@swu.edu.cn; liuzuliankl@163.com; xiang_shine@foxmail.com

Consequently, nitrogen conversion efficiency in the silk glands is remarkably high (Horie & Watanabe, 1986). Beyond silk synthesis, the silkworm employs an additional strategy to regulate nitrogen homeostasis. Excess amino acids are incorporated into the cocoon, reducing the risk of aminoacidemia and supporting larval survival (Hirayama et al., 1996, 1997). This mechanism is particularly critical for metamorphosis in species with high silk output, such as *B. mori*. Additionally, both silk proteins and the silk glands themselves serve as nitrogen reservoirs for later developmental stages. Following cocoon construction, the silk glands undergo programmed cell death, initiating degradation processes that release stored nutrients (Goncu & Parlak, 2008; Kawamoto et al., 2014; Li et al., 2016; Lőrincz & Juhász, 2020; Montali et al., 2017). These nutrients are subsequently reallocated to support tissue remodeling during metamorphosis and sustain development through pupation and adult emergence (Wang et al., 2016). The biological processes governing silk gland function, including endoreplication, silk protein synthesis, autophagy, and apoptosis, represent a finely tuned trade-off between the ecological benefits of silk production and the metabolic constraints of nitrogen reallocation during metamorphosis. Disruptions in this system can interfere with silk gland degradation, impair programmed cell death, and hinder metamorphic progression (Cui et al., 2018; Ye et al., 2021).

Recent evolutionary genomic analyses revealed strong signatures of artificial selection in genes related to nitrogen mobilization, including glutamine synthetase (*GS*), glutamate synthetase (*GOGAT*), asparagine synthetase (*AS*), and glutamate dehydrogenase (*GDH*), during the domestication of *B. mori* (Tong et al., 2022; Xiang et al., 2018), with glutamate oxaloacetate transaminase 1 (*GOT1*) also implicated in the genetic improvement of the species (Xiang et al., 2018). Notably, knockout of *GOGAT* and *AS* resulted in similarly deficient cocoon production and disrupted metamorphosis (Xiang et al., 2018), underscoring the critical role of nitrogen mobilization genes in orchestrating silk production, silk gland biology, and developmental transitions. However, despite these insights, the precise molecular mechanisms underlying their functions remain elusive (Hirayama et al., 1997; Hirayama & Nakamura, 2002; Xiang et al., 2018).

These domestication-associated genes play key roles in glutamate (Glu) and aspartate (Asp) metabolism, particularly in the consumption and anaplerosis of tricarboxylic acid (TCA) cycle intermediates such as α-ketoglutarate (α-KG). Specifically, GS catalyzes the adenosine triphosphate (ATP)-dependent condensation of Glu and ammonia to form glutamine, while GOGAT facilitates the reductive transfer of the amide group from glutamine to α-KG, producing two Glu molecules. AS transfers the amide group from glutamine (Gln) to Asp, producing asparagine (Asn) and Glu. GDH catalyzes the reversible conversion of Glu to α-KG and ammonia, using NADP(H) and NAD(H) as cofactors, though it typically favors the oxidative deamination of Glu (Melo-Oliveira et al., 1996). In contrast to these nitrogen mobilization enzymes, *GOT1*, a gene associated with silkworm improvement, catalyzes the reversible conversion of Glu and oxaloacetate (OAA) into α-KG and Asp, thus coordinating both carbon and nitrogen metabolism, a function conserved across many organisms (Coloff et al., 2016).

Although these genes are functionally interconnected within the amino acid metabolism and share catalytic relationships, their specific roles in the Glu and Asp metabolic pathways, as well as the distinct reactions they mediate, remain differentiated. However, the extent of their interactions, the mechanisms by which they regulate downstream signaling pathways, and their collective influence on cocoon production, silk gland function, and metamorphosis are not well understood. In this study, CRISPR/Cas9-mediated knockouts of domestication- and improvement-associated nitrogen mobilization genes were generated in *B. mori* to investigate their roles in silk gland function and development. Comparative phenotypic analyses revealed both consistent and gene-specific effects on cocoon production, silk gland physiology, and metamorphosis. Transcriptomic profiling of silk glands uncovered distinct regulatory mechanisms governing these genes and their functional interactions. Notably, a previously unrecognized link between nitrogen mobilization and autophagy in silk glands was identified. These findings offer new perspectives on the metabolic regulation of silk gland biology and its broader impact on silkworm development.

MATERIALS AND METHODS

Silkworm strains

The multivoltine, non-diapausing silkworm strain Nistari was used in this study. Larvae were reared on fresh mulberry leaves under standard conditions at 25℃ and 40%–60% relative humidity.

Plasmid construction and silkworm germline transformation

A binary transgenic CRISPR/Cas9 system was used to construct loss-of-function mutants for *GS*, *GOGAT*, *AS*, *GDH*, and *GOT1* (Xu et al., 2017). The nos-Cas9 transgenic silkworm line (nos-Cas9/IE1-EGFP), which expresses the Cas9 protein under the control of the *B. mori nanos* promoter, was previously established (Xu et al., 2019). To target these five genes, several pBac[IE1-DsRed2-U6-sgRNAs] (U6-sgRNA/IE1-DsRed) plasmids were constructed. Each U6-sgRNA plasmid contained two site-specific single-guide RNAs (sgRNAs) driven by two *U6* promoters, while the DsRed fluorescent protein, used for screening, was expressed under the control of the *IE1* promoter. Primer sequences used for plasmid construction and sgRNA targeting are listed in Supplementary Table S1.

For silkworm germline transformation, preblastodermal embryos were prepared and microinjected with transgenic plasmids (400 ng/μL) together with helper plasmids (200 ng/μL) and subsequently incubated in a humidified chamber at 25℃ for 10–12 days until hatching (Tan et al., 2013). Larvae were reared with fresh mulberry leaves under standard conditions. Putative transgenic generation 0 (G0) moths were sib-mated or backcrossed with wild-type (WT) moths, and G1 progeny were screened during early larval stages using fluorescence microscopy (Nikon AZ100, Japan) based on the red fluorescent marker. The nos-Cas9 and U6-sgRNA lines were crossed to generate *GS*, *GOGAT*, *AS*, *GDH*, and *GOT1* mutants, yielding transgenic individuals carrying both EGFP and DsRed fluorescence markers for subsequent experiments.

Mutagenesis analysis

Genomic DNA was extracted from three randomly selected mutants at the larval stage using standard SDS lysis-phenol

treatment. Samples were incubated with proteinase K at 56℃ for 5 h, followed by RNase treatment, and purified for mutagenesis analysis via polymerase chain reaction (PCR) amplification with specific primers (Supplementary Table S1). For each gene mutant, total RNA was extracted from the whole bodies of three randomly selected individuals at the prepupal stage. The RNA was then reverse-transcribed into cDNA, which served as the template for reverse transcription-quantitative real-time polymerase chain reaction (RT-qPCR).

RNA isolation, cDNA synthesis, and RT-qPCR

Total RNA was extracted from three individual mutants or WT animals using TRIzol reagent (YEASEN, China), following the manufacturer's instructions. RNA quality was confirmed by agarose gel electrophoresis. A 1 μg aliquot of total RNA was treated with gDNA eraser and used to synthesize cDNA with a PrimeScript™ RT Reagent Kit (Takara, Japan). RT-qPCR analysis was performed using SYBR Green Real-time PCR Master Mix (Toyobo, Japan) on the StepOnePlus Real-Time PCR system (Applied Biosystems) to quantify the relative abundance of selected transcripts. The *B. mori ribosomal protein 49* (*RP49*) gene was used as an internal control to normalize variations across different templates. Each RT-qPCR experiment was conducted with three independent biological replicates. The amplification conditions were as follows: incubation at 95℃ for 5 min, followed by 40 cycles at 95℃ for 15 s and 60℃ for 1 min. All primers used for RT-qPCR are listed in Supplementary Table S1.

Analysis of commercially important silk-related traits

Larval body weights were measured on day 2 of the fourth instar and day 3 of the fifth instar. Pupal and cocoon weights were measured on days 5–6 of the pupal stage. Each experimental group consisted of at least 20 individuals (n>20).

RNA sequencing (RNA-seq) and data analyses

For RNA-seq, silk glands were dissected from three biological replicates of both WT and mutant individuals at the prepupal stage. Samples were immediately flash-frozen on dry ice and sent to Novogene (China) for RNA extraction and sequencing. Sequencing libraries were generated using a NEBNext® Ultra™ RNA Library Prep Kit for Illumina® (New England Biolabs, USA), with index codes assigned to each sample following the manufacturer's recommendations. Library clustering was performed on a cBot Cluster Generation System using a HiSeq 4000 PE Cluster Kit (Illumina, USA), and sequencing was conducted using the Illumina Hiseq 4000 platform (Illumina, USA). Raw sequencing reads were processed for quality control, filtering, and alignment. Transcript abundance was quantified by quasi-mapping raw reads to the silkworm reference gene set (https://silkdb.bioinfotoolkits.net/base/download/-1) using Salmon (v.1.9.0). Gene-level counts were obtained using tximport and further normalized using DEseq2 (v.1.34.0) in the R (Love et al., 2014; Patro et al., 2017; Soneson et al., 2015). Differentially expressed genes (DEGs) were identified using DESeq2 based on corrected P<0.05 and $|\text{Log}_2\text{fold change}|\geq 1$ criteria. Transcript abundance for each gene was expressed in transcripts per million (TPM). Kyoto Encyclopedia of Genes and Genomes (KEGG) pathway enrichment analyses were conducted using the OmicShare online platform (https://www.omicshare.com/tools/), with all expressed DEGs (TPM>1) in the silk glands used as the background reference. Pathways with adjusted P<0.05 were considered significantly enriched. The P-adjust value represents the P-value from the hypergeometric test after multiple testing correction.

LysoTracker green staining

Posterior silk glands (PSGs) from *AS* mutants and WT individuals at the prepupal stage were dissected, thoroughly washed with phosphate-buffered saline (PBS, 0.1 mol/L, pH 7.0), and incubated for 30 min at 37℃ in a staining solution containing Hoechst (C1011, Beyotime, China) and LysoTracker Green DND-26 (L7526, 50 nmol/L, Invitrogen, USA). After incubation, samples were washed three times with PBS. Confocal imaging was performed using an FV3000 confocal microscope (Olympus, Japan). Three independent biological replicates were conducted.

Enzymatic activity assays for nitrogen mobilization

GDH and GOT activities were determined using commercial assay kits manufactured by Beijing Boxbio Science & Technology Co., Ltd. (AKAM005M, AKAM019M, China). AS activity was determined using a commercial assay kit manufactured by Shanghai Crystal Antibiotic Engineering Co., Ltd. (JKSW-E13960, China).

Gene co-expression network analysis

Co-expression networks were constructed using the R package WGCNA (v.1.47) (Langfelder & Horvath, 2008) by integrating DEGs identified in *ΔGS*, *ΔGOGAT*, *ΔAS*, and *ΔGOT1* compared with their respective controls. Network construction and module detection were performed using stepwise network construction and module detection. The adjacency matrix for weighted gene co-expression networks was calculated by selecting an appropriate thresholding power using the "pickSoftThreshold" function in the WGCNA package. Modules were identified using default settings, and a visual representation of the network was constructed using Cytoscape (v.3.9.1) (Shannon et al., 2003).

Statistical analysis

All experiments were conducted with at least three biological replicates. All data are presented as mean±standard error of the mean (SEM). Differences between groups were examined using either two-tailed Student's t-test or two-way analysis of variance (ANOVA). All statistical analyses and graphical representations were performed using GraphPad Prism v.10.

RESULTS

Distinct temporal and spatial expression patterns of *GS*, *GOGAT*, and *AS* compared to *GDH* and *GOT1* during silkworm development

The temporal expression profiles of five nitrogen mobilization-related genes from the embryonic stage (E) to day 3 of the pupal stage (P3) revealed distinct regulatory patterns. *GS* and *GOGAT* exhibited highly synchronized expression dynamics, with a significant increase on the fifth day of the fifth instar (L5D5). Similarly, *AS* displayed relatively elevated expression during the later stages of the fifth instar, peaking at P1 (Figure 1A). In contrast, *GDH* maintained consistently high expression across all tested larval and pupal stages, except during the third instar, when *GOT1* exhibited a transient surge. The expression of *GOT1* increased steadily throughout the early larval stages, peaking on the second day of the fourth instar (L4D2), before declining sharply in the fifth instar and wandering stages. These findings imply that *GOT1* may play a more prominent role in early larval development rather than

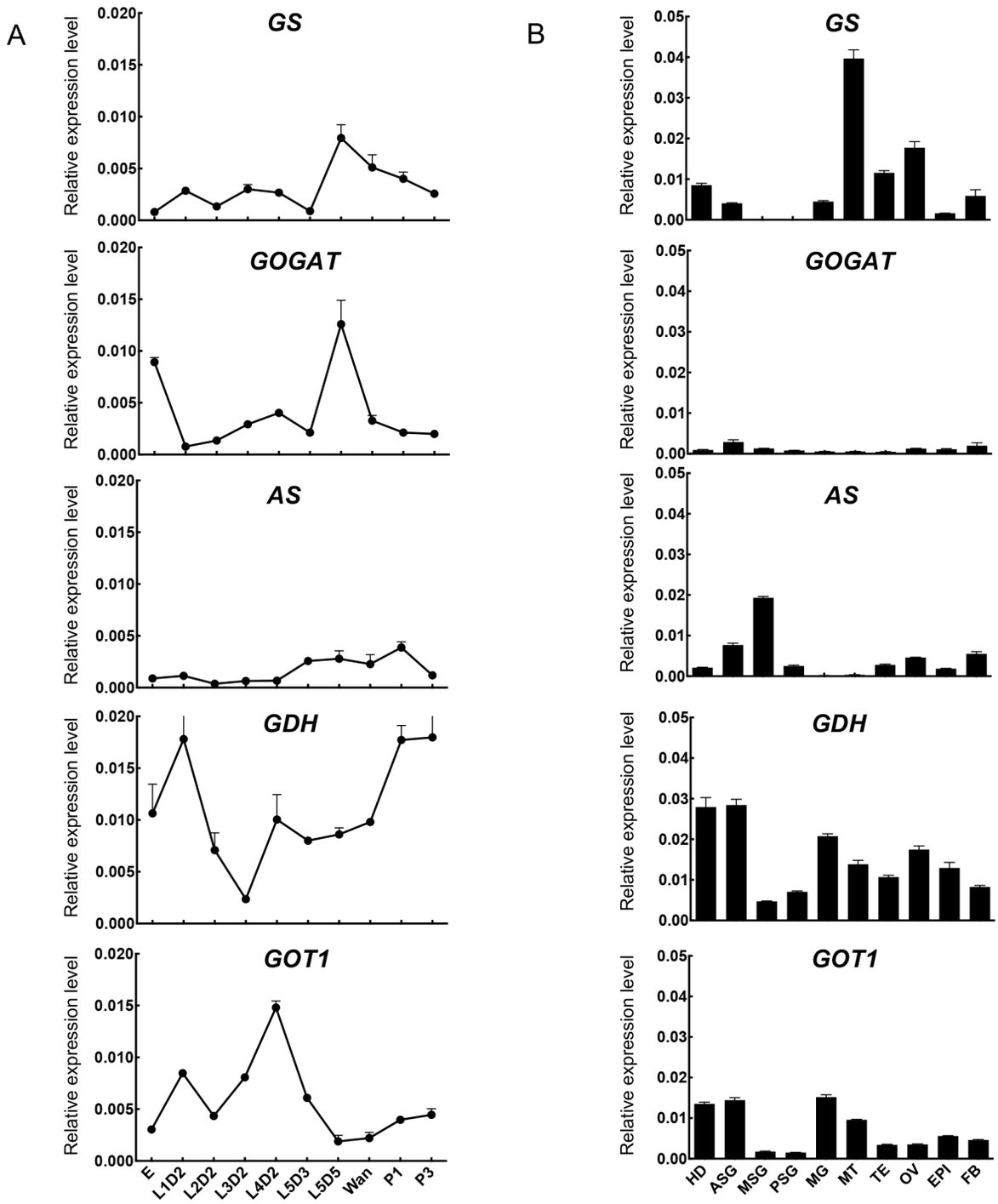

Figure 1 Temporal and spatial expression of nitrogen mobilization-related domestication and improvement genes in the silkworm

A, B: Relative mRNA expression levels of *GS*, *GOGAT*, *AS*, *GDH*, and *GOT1* at 10 different stages (A) and 10 tissues at day three of the fifth instar stage (L5D3) (B) via RT-qPCR analysis. Stages tested included embryo (E), day two of the first instar (L1D2), day two of the second instar (L2D2), day two of the third instar (L3D2), day two of the fourth instar (L4D2), L5D3, day five of the fifth instar (L5D5), day one of the pupal stage (P1), and day three of the pupal stage (P3). Tissues tested included head (Hd), anterior silk gland (ASG), middle silk gland (MSG), posterior silk gland (PSG), midgut (MG), Malpighian tubule (MT), testis (TE), ovary (OV), epidermis (EPI), and fat body (FB). mRNA levels were normalized to levels of *B. mori* ribosomal protein 49 (*RP49*).

silk production.

Given that the third day of the fifth instar (L5D3) represents a critical stage for silk gland maturation (Ma et al., 2024), tissue-specific expression patterns of these five genes were analyzed at this time point (Figure 1B; Supplementary Figure S1). *GS* and *GOGAT* exhibited distinct tissue distributions: *GS* was highly expressed in the Malpighian tubules but was almost undetectable in the silk glands, indicating its primary role in ammonia detoxification during nitrogen metabolism. In contrast, *GOGAT* displayed relatively low expression across tissues, with only slight expression detected in the silk glands. *AS* showed markedly higher expression in the silk glands, suggesting its essential role in silk gland function. Furthermore, *GDH* and *GOT1* were broadly expressed across

multiple tissues but were expressed at relatively lower levels in the silk glands (Figure 1B; Supplementary Figure S1). These findings suggest that *GDH* and *GOT1* contribute more significantly to overall silkworm metabolism and development rather than being directly involved in silk protein synthesis.

Disruption of *GS*, *GOGAT*, *AS*, *GDH*, and *GOT1* impairs silkworm larval growth with varying degrees of severity

To evaluate the physiological roles of nitrogen mobilization-related genes in silk protein synthesis, a binary transgenic CRISPR/Cas9 system was employed to establish somatic mutants for *GS*, *GOGAT*, *AS*, *GDH*, and *GOT1*, labeled as *ΔGS*, *ΔGOGAT*, *ΔAS*, *ΔGDH*, and *ΔGOT1*, respectively (Supplementary Figure S2A) (See Methods). PCR-based genotyping of the target genomic regions in three randomly selected G1 offspring from each mutant line confirmed the presence of large fragment deletions (Supplementary Figure S2B), disrupting the coding sequences. Furthermore, RT-qPCR further validated significant reductions in mRNA levels for the respective target genes in all mutant lines compared with WT individuals (Supplementary Figure S2C).

All *GS*, *GOGAT*, *AS*, *GDH*, and *GOT1* mutants successfully hatched but exhibited severe larval growth impairments (Figure 2A), with significantly lower body weights than WT individuals (Figure 2B). Growth retardation was evident in all mutant lines, although *ΔGS* and *ΔGOGAT* exhibited relatively milder delays compared with *ΔAS*, *ΔGDH*, and *ΔGOT1* (Figure 2C). In addition, all mutants displayed a marked decline in survival (1.7%–47.5%) relative to WT (93.0%), with the strongest decline observed in *ΔGDH* (1.7%) and milder declines in *ΔGS* (18.0%) and *ΔGOGAT* (47.5%) (Figure 2D). A notable reduction in *ΔGS* survival occurred during the fifth instar (Figure 2D). While *ΔAS* and *ΔGOT1* exhibited similar survival rates at the end of the fifth instar (7.0% and 6.5%, respectively), *GOT1* mutants began experiencing mortality earlier, with a significant increase in deaths at the third instar, whereas *ΔAS* displayed a sharp reduction in survival at the fourth instar. This suggests that *GOT1* exerts its functional effects earlier in development than *AS* (Figures 1, 2D). Due to the extremely low survival of *ΔGDH* beyond the wandering and pupal stages, *ΔGDH* was excluded from further in-depth analyses.

Disruption of *GS*, *GOGAT*, *AS*, and *GOT1* consistently reduces cocoon and pupal weight but differentially affects silk gland biology and silk protein gene transcription

All *GS*, *GOGAT*, *AS*, and *GOT1* mutants exhibited severe developmental impairments, including the production of significantly smaller cocoons, metamorphosis arrest, and eventual mortality (Figure 3A). Among these, *ΔGS* displayed the most severe phenotype, forming only a thin silk layer rather than a fully developed cocoon (Figure 3A), emphasizing

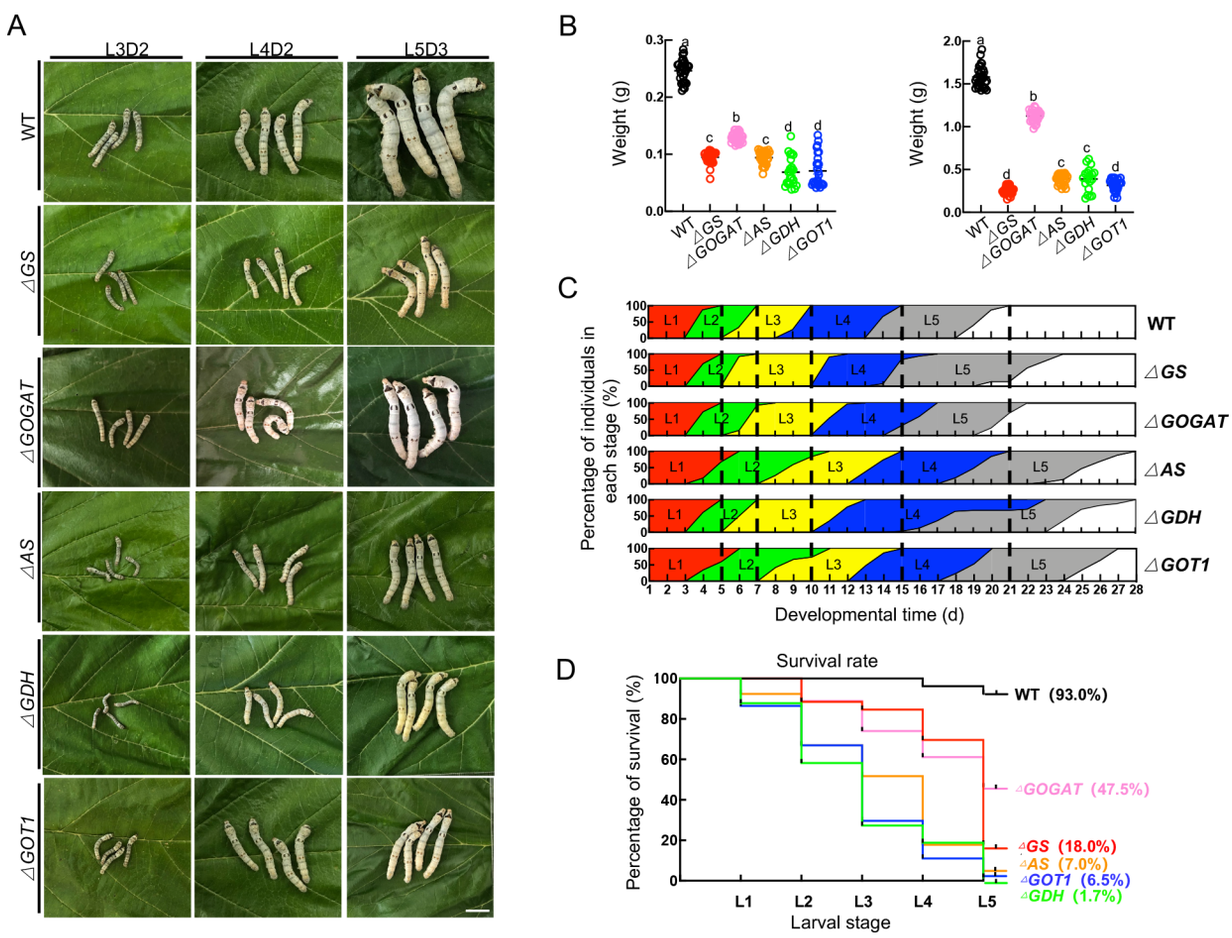

Figure 2 Loss-of-function in *GS*, *GOGAT*, *AS*, *GDH*, and *GOT1* leads to impaired development in silkworm larvae

A, B: Knockout of *GS*, *GOGAT*, *AS*, *GDH*, and *GOT1* induces smaller body size (A) and lower body weights (B) in the larval stage. C: Larval developmental stages in mutants and wild-type (WT) individuals. L1–L5 stages are marked in red, green, yellow, blue, and gray sequentially through developmental timeline. Curves between different stages show molting ratio. All mutants showed delayed development periods. D: Survival rate analysis of mutants and WT individuals. All mutants exhibited high mortality during the larval stage.

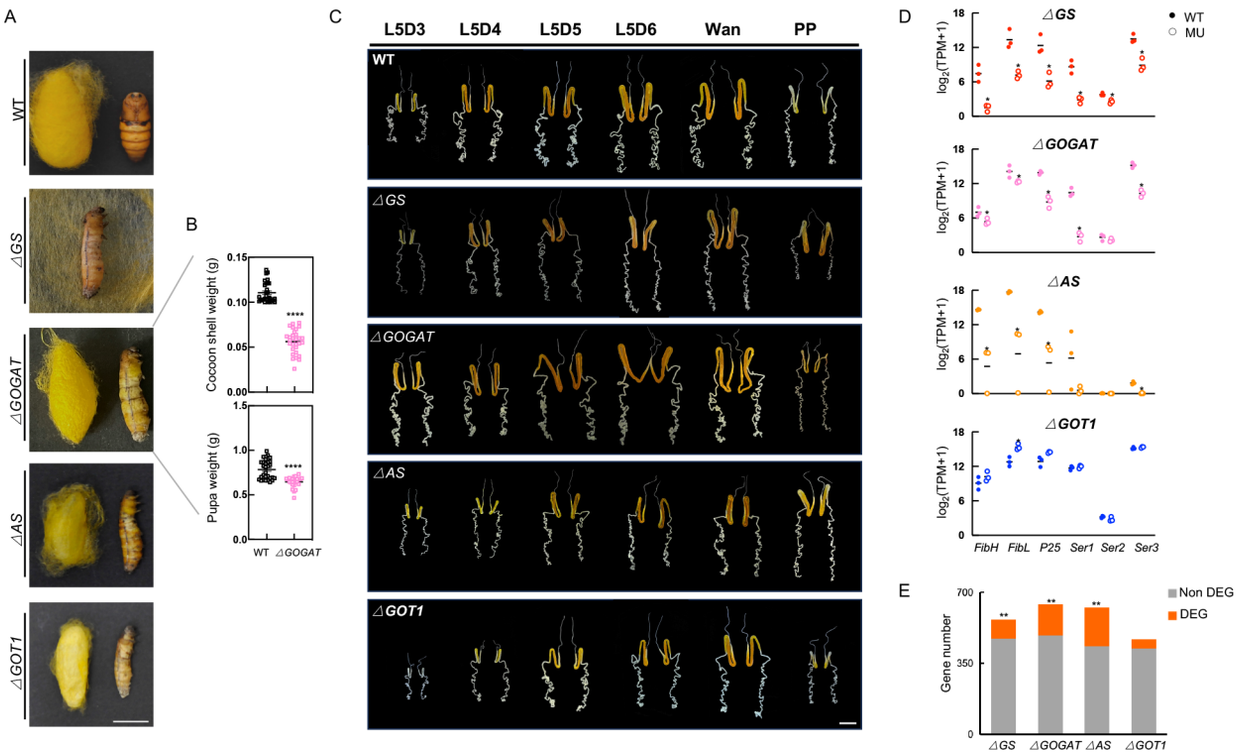

Figure 3 Silk production-related phenotypes of *GS*, *GOGAT*, *AS*, and *GOT1* mutants

A: Representative images of cocoons and pupation phenotypes between WT individuals and *GS*, *GOGAT*, *AS*, and *GOT1* mutants. All mutants exhibited reduced silk production and failed to reach adulthood. Scale bar: 1 cm. B: Cocoon and pupal weights between WT individuals and *GOGAT* mutants. ns: Not significant; *: $P<0.05$; **: $P<0.01$; ***: $P<0.001$; ****: $P<0.0001$. C: Representative images of dissected silk glands at six different stages: L5D3, day four of the fifth instar (L5D4), L5D5, wandering stage (Wan), and prepupal stage (PP) between WT individuals and mutants. Scale bar: 1 cm. D: Expression levels (TPM) of fibroin heavy chain (*fib-H*), fibroin light chain (*fib-L*), fibrohexamerin (*P25*), sericin1 (*Ser1*), sericin2 (*Ser2*), and sericin3 (*Ser3*) in silk glands of mutants and controls at the prepupal stage. Asterisk (*) represents differentially expressed genes (DEGs). E: Differentially expressed and expressed transcription factors in silk gland of mutants and controls. ns: Not significant; *: $P<0.05$; **: $P<0.01$; ***: $P<0.001$; ****: $P<0.0001$.

its critical role in silk production. Similarly, *AS* mutants also produced notably thinner cocoons. In contrast, *GOGAT* mutants displayed a relatively milder phenotype, making it suitable for further analysis of cocoon layer weight and pupal weight, both of which were significantly reduced compared to the WT individuals (Figure 3B).

To further investigate the role of these genes in silk gland biology during the late larval and prepupal stages, silk gland morphology was examined across mutant lines (Figure 3C). In *GOGAT* mutants, silk glands were noticeably enlarged before the onset of silk spinning but became markedly smaller in metamorphosis-arrested prepupae. However, these small silk glands did not exhibit the typical degradation pattern observed in WT silk glands, which fade significantly during this stage. *GS* and *AS* mutants exhibited slightly smaller silk glands prior to silk spinning but showed a pronounced delay in silk gland programmed cell death, with the delay being most severe in *ΔAS*. Despite the distinct effects on silk gland morphology, *ΔGS*, *ΔGOGAT*, and *ΔAS* consistently displayed severely reduced transcription of silk protein genes (Figure 3D). In contrast, *GOT1* mutants had smaller silk glands both before and after silk spinning but showed no significant differences in silk protein gene expression (Figure 3D).

Silk yield and silk gland development during metamorphosis are tightly regulated by the expression of silk protein genes (Cui et al., 2018; Ye et al., 2021). Under normal conditions, the core silk fibroin genes (*fib-H* and *fib-L*) are up-regulated at the prepupal stage, whereas sericin genes (*Ser1*, *Ser2*, and *Ser3*) are down-regulated compared to the end larval stage (Supplementary Figure S3A). The higher transcription levels of fibroin genes in prepupae likely reflect their critical roles in amino acid sequestration. The expression of silk protein genes, as well as silk gland function during silk spinning and metamorphosis, is governed by a complex regulatory network involving multiple transcription factors. As expected, compared to the WT controls, a significantly larger proportion of differentially expressed transcriptional factors were found in *ΔGS*, *ΔGOGAT*, and *ΔAS* than in *ΔGOT1* (Figure 3E). These results further demonstrate that *GS*, *GOGAT*, and *AS* have distinct regulatory functions compared to *GOT1* in controlling silk protein genes expression and silk gland biology during *B. mori* metamorphosis.

Comparative transcriptome analysis reveals shared and distinct downstream pathways of *GS*, *GOGAT*, and *AS* in *B. mori* silk glands

To elucidate the molecular mechanisms underlying the functional roles of *GS*, *GOGAT*, *AS*, and *GOT1* in silk gland biology during silkworm metamorphosis, a comparative transcriptome analysis was performed on silk glands from metamorphosis-arrested mutants and WT individuals at the prepupal stage. The number of DEGs in *ΔGOT1* was significantly lower (906) than in *ΔGS*, *ΔGOGAT*, and *ΔAS* (1 998–3 652) (Figure 4A), suggesting that *GOT1* has a more limited role in regulating silk gland biology during metamorphosis. Moreover, a substantial number of shared

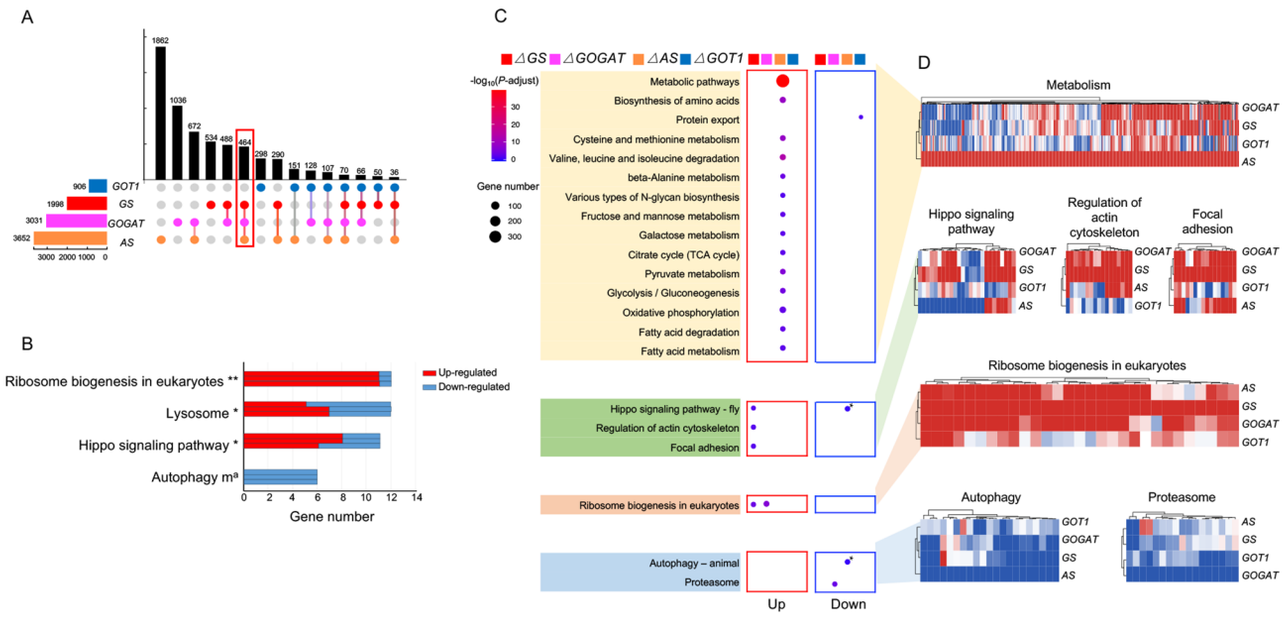

Figure 4 Comparative analysis of silk gland transcriptome between *GS*, *GOGAT*, *AS*, and *GOT1* mutants and their controls

A: UpSet Venn diagram of DEGs of four comparisons, i.e., four mutants vs. their controls. B: Functional enrichment analysis of common DEGs of *ΔGS*, *ΔGOGAT*, and *ΔAS*. For each pathway, from top to bottom, *ΔGS*, *ΔGOGAT*, and *ΔAS*, respectively. Horizontal coordinate represents number of genes enriched in this pathway, with red representing up-regulated genes and blue representing down-regulated genes. Asterisk (*) indicates significantly enriched pathways, while m^a denotes marginally significant enrichment. C: Representative pathways significantly enriched in up- and down-regulated DEGs in *ΔGS*, *ΔGOGAT*, *ΔAS*, and *ΔGOT1*. All pathways had adjusted P<0.05. Asterisk (*) indicates marginally significant enrichment. D: Heatmap and hierarchical clustering analysis of genes enriched in pathways in (C) between controls and mutants using $\log_2$fold change values of TPM.

DEGs were observed among *ΔGS*, *ΔGOGAT*, and *ΔAS*, whereas *ΔGOT1* shared relatively few DEGs with these three mutants (Figure 4A). A set of 464 DEGs common to *ΔGS*, *ΔGOGAT*, and *ΔAS* were significantly enriched in pathways such as the Hippo signaling pathway, ribosome biogenesis in eukaryotes, lysosomal function, and autophagy (Figure 4B), suggesting that these genes are functionally linked to these regulatory processes.

To further investigate the transcriptional changes associated with each mutant, DEGs were analyzed for each WT-mutant pair. Prior to this, gene expression dynamics in silk glands during normal silkworm metamorphosis were examined (Supplementary Figure S3). At the prepupal stage, silk glands exhibited significant up-regulation of pathways involved in organ size regulation, including Hippo signaling, Ras signaling, and actin cytoskeleton remodeling, as well as autophagy activation (Supplementary Figure S3C, D). In contrast, pathways related to material and energy metabolism, such as the TCA cycle, carbon metabolism, amino acid biosynthesis, protein export, ribosome biogenesis, and oxidative phosphorylation, were all down-regulated (Supplementary Figure S3C, D).

Next, transcriptomic alterations in silk glands were analyzed for each mutant (Supplementary Table S2). In *GOT1* mutants, only the protein export pathway was significantly down-regulated, which also showed reduced expression during normal metamorphosis (Figure 4C; Supplementary Figure S3C). The expression of DEGs associated with key regulatory pathways in *ΔGS*, *ΔGOGAT*, and *ΔAS* remained largely unchanged in *ΔGOT1*, suggesting a relatively minor impact on the silk gland transcriptome. In contrast, *AS* mutants exhibited the most pronounced transcriptomic disruptions in metamorphosis-arrested prepupal silk glands. Notably, the direction of gene expression changes in *ΔAS* was almost entirely opposite to that observed during normal metamorphosis. *ΔAS* silk glands displayed an abnormal up-regulation of metabolic pathways, including carbohydrate metabolism (TCA cycle and pyruvate metabolism), amino acid metabolism (cysteine and methionine metabolism, beta-alanine metabolism), and fatty acid metabolism (fatty acid degradation) (Figure 4C). Pathways involved in organ size regulation, such as Hippo signaling and autophagy, were significantly down-regulated. To confirm impaired autophagy in *ΔAS*, LysoTracker staining was performed, revealing a marked reduction in autophagosome and autolysosome formation (Figure 5). *ΔGS* and *ΔGOGAT* exhibited significant up-regulation of genes involved in ribosome biogenesis (Figure 4C, D). Additionally, *ΔGS* showed strong up-regulation of pathways associated with organ size regulation, including Hippo signaling, actin cytoskeleton regulation, and focal adhesion (Figure 4C). In *ΔGOGAT*, proteasome pathway genes were significantly down-regulated.

Heatmap analysis of DEGs enriched in key metabolic pathways revealed a striking overrepresentation of up-regulated genes in *AS* mutants (Figure 4D). Genes associated with the Hippo signaling pathway, however, exhibited contrasting expression patterns, with significant down-regulation in *ΔAS*, full up-regulation in *ΔGS*, and partial up-regulation in *ΔGOGAT*. Detailed mapping of DEGs within the Hippo signaling pathway demonstrated profound divergence in expression directions in *ΔAS* compared to *ΔGS* and *ΔGOGAT* (Supplementary Figure S4). Genes normally up-regulated in silk glands during the prepupal stage were completely repressed in *ΔAS*, including *Yorkie* (*yki*), a critical Hippo pathway regulator (Supplementary Figure S4A, B). In contrast, a substantial subset of these genes were abnormally up-

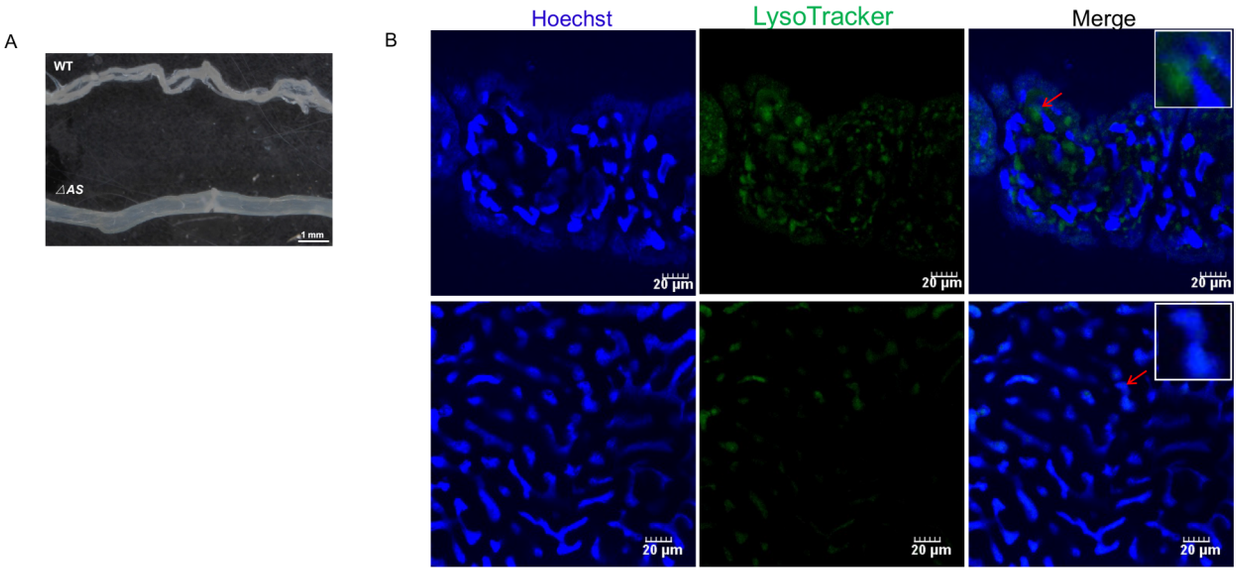

Figure 5 Mutation of *AS* impaired autophagy in silk glands

A: Posterior silk gland (PSG) of *ΔAS* and WT individuals at the prepupal stage. B: LysoTracker green staining of PSG from *ΔAS* and WT individuals.

regulated in *ΔGS* and *ΔGOGAT*, although *yki* was not differentially expressed in either of these mutants (Supplementary Figure S4A). Pathways associated with organ size regulation, such as actin cytoskeleton remodeling and focal adhesion, were fully up-regulated in *ΔGS*, partially up-regulated in *ΔGOGAT*, and unchanged in *ΔAS*. Genes involved in ribosome biogenesis were fully up-regulated in *ΔGS* but only partially up-regulated in *ΔGOGAT* and *ΔAS* (Figure 4D). Notably, ribosome biogenesis was not significantly enriched in *ΔAS*, suggesting that the predominant transcriptomic alterations in *ΔAS* may be attributed to abnormally activated metabolic pathways. Genes associated with autophagy were broadly down-regulated in *ΔAS*, with partial down-regulation also observed in *ΔGOGAT* and *ΔGS* (Figure 4D). These findings strongly suggest that distinct molecular mechanisms underlie the observed disruption of silk gland programmed cell death in these mutants.

Pathway crosstalk mediated by nitrogen mobilization-related genes in *B. mori* silk glands

Given the interconnected catalytic roles of nitrogen mobilization-related enzymes, potential pathway crosstalk in silk glands was examined by analyzing mRNA expression changes and enzymatic activity in the mutant lines. *ΔGS* and *ΔGOGAT*, which disrupted the GS/GOGAT cycle, both showed significant up-regulation of *AS* and *GDH* mRNA expression in silk glands. However, only *GOGAT* mutants displayed a corresponding increase in enzyme activity (Figure 6). In *ΔAS*, both *GOT1* mRNA and enzymatic activity were significantly elevated, whereas *ΔGOT1* showed no differential expression of these genes (Figure 6).

To further explore the crosstalk among nitrogen metabolism pathways and their regulatory effects on silk gland biology during metamorphosis, gene co-expression networks were constructed. All DEGs were categorized into 16 modules (Figure 7A; Supplementary Figure S5). The M1 module was significantly up-regulated in both *GS* and *GOGAT* mutants (Figure 7A), suggesting a high degree of functional consistency between these genes. As expected, genes in the M1 module were significantly enriched in ribosome biogenesis, a pathway commonly up-regulated in both *ΔGS* and *ΔGOGAT* (Figure 7B). A subnetwork was constructed using DEGs from *ΔGS* and *ΔGOGAT* in the M1 module, revealing consistent up-regulation of all genes within this cluster. Notably, two key nitrogen mobilization genes, *AS* and *GDH*, were also positioned within this subnetwork, closely associated with genes involved in ribosome biogenesis and further linked to the Hippo signaling pathway. These results suggest that the up-regulation of *AS* and *GDH* may play a key role in coordinating organ size regulation through Hippo signaling and enhancing protein synthesis via ribosome biogenesis (Figure 7C). In *ΔGS*, activation of these pathways was further connected to additional organ size regulatory pathways, an association that was not observed in *ΔGOGAT*. Instead, *ΔGOGAT* exhibited a distinct regulatory link, characterized by up-regulation of spliceosome-related genes (Figure 7C).

The M3 module was significantly up-regulated in *ΔAS* (Figure 7A), highlighting its functional association with AS activity. Genes within M3 were predominantly enriched in metabolic pathways (Figure 7B), consistent with those up-regulated in *ΔAS* (Figure 4C). Subnetwork analysis of DEGs in *ΔAS* within the M3 module unexpectedly identified the mitochondrial homolog of *GOT1* (*GOT2*), which was closely associated with metabolic genes (Figure 7D). Increased *GOT* expression leads to the production of OAA, a critical intermediate in the TCA cycle, potentially driving enhanced carbohydrate metabolism. Additionally, the resulting Glu could participate in transamination reactions, facilitating the synthesis of various other amino acids and further promoting metabolic activity. Although ribosome biogenesis-related genes were also up-regulated in *ΔAS* (Figure 4D), co-expression network analysis could not explain the underlying mechanism.

DISCUSSION

Nitrogen is a vital yet limited resource for the growth and development of all organisms, particularly for plants and herbivorous animals. As a silk-producing insect, *B. mori* has evolved a highly efficient nitrogen mobilization system during domestication. The silk gland plays a pleiotropic role in

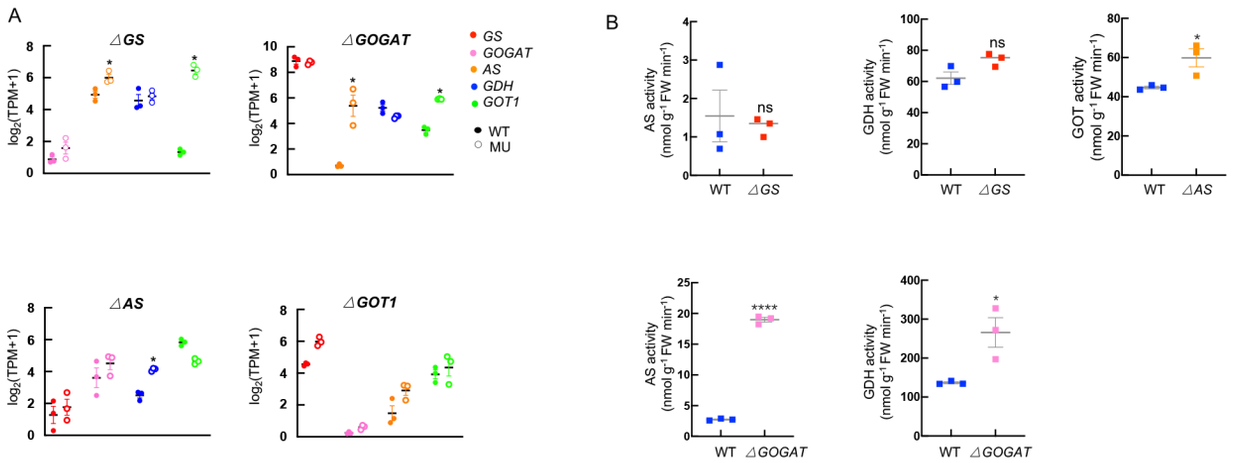

Figure 6 Effects of loss-of-function of nitrogen mobilization-related enzymes on other components

A: Expression levels (TPM) of *GS*, *GOGAT*, *AS*, *GDH*, and *GOT1* in *ΔGS*, *ΔGOGAT*, *ΔAS*, and *ΔGOT1* silk glands. Asterisk (*) represents DEGs. B: Enzymatic activities of AS and GDH in the silk glands of *ΔGS* and *ΔGOGAT* and GOT in the silk glands of *ΔAS* at the prepupal stage. ns: Not significant; *: P<0.05; **: P<0.01; ***: P<0.001; ****: P<0.0001.

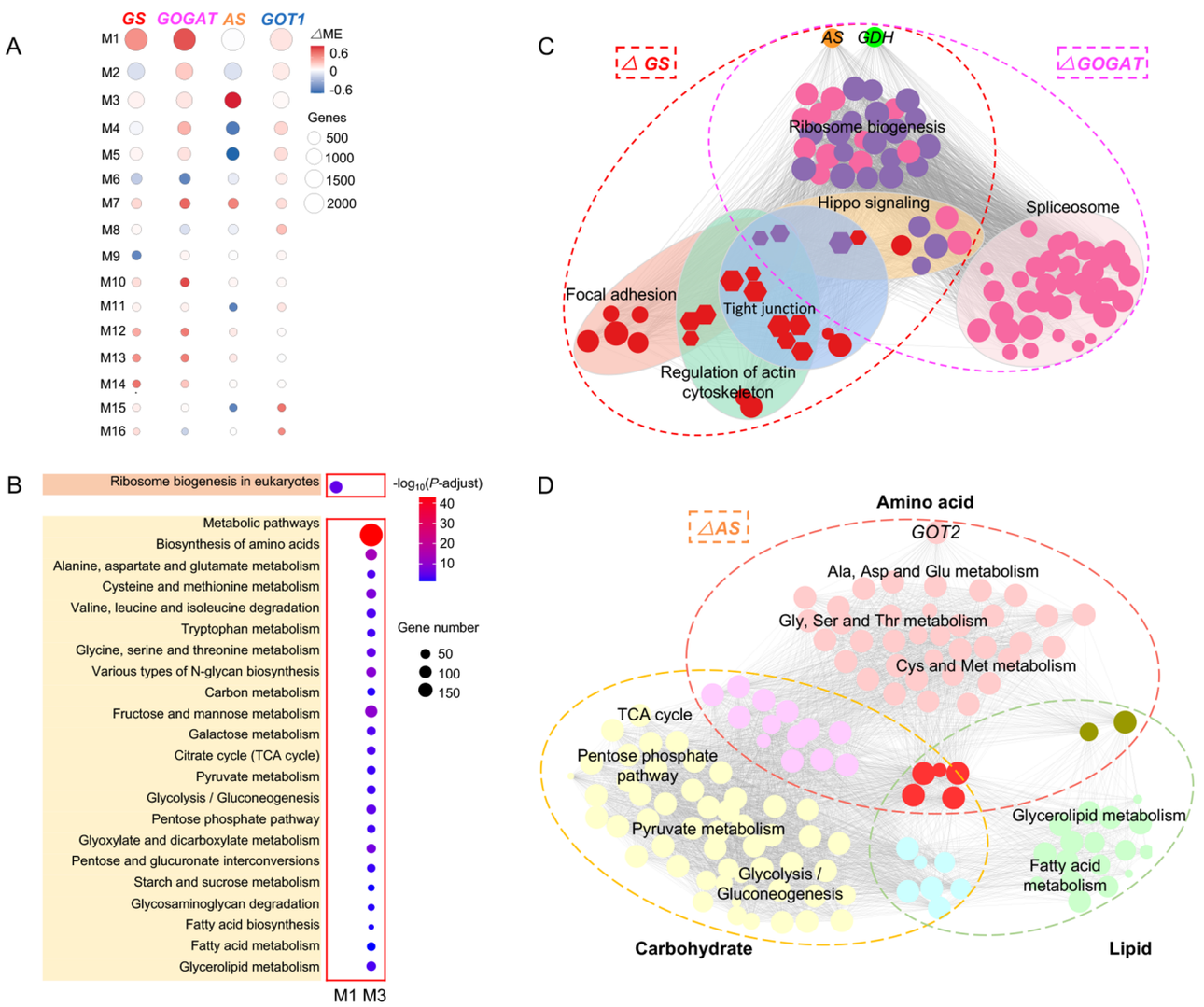

Figure 7 Co-expression network analysis and identification of key modules associated with *GS*, *GOGAT*, and *AS*

A: Module-mutant module eigengene (ME) bubble map. Color indicates difference between mean ME of the module in each mutant and that of its control, while circle size corresponds to the number of genes. B: Functional enrichment analysis of genes in M1 and M3 modules. C, D: Co-expression network of DEGs in *ΔGS* and *ΔGOGAT* in M1 (C) and DEGs in *ΔAS* in M3 module (D). Representative pathways are highlighted in (D). All genes in the two networks were up-regulated. Common genes shared by pathways are marked in hexagons, while others are marked in ellipses.

recruiting nitrogen resources for silk production, mitigating the risk of aminoacidemia through fixing free amino acids (Hirayama et al., 1996, 1997), and contributing to nitrogen reallocation for metamorphosis through programmed cell death. However, the precise contribution of nitrogen mobilization genes to this complex process remains enigmatic. This study systemically investigated the functional roles of these genes in silkworm development and metamorphosis, providing critical insights into their regulatory influence on silk gland biology.

Our findings indicated that the typical ammonia re-assimilation genes *GS* and *GOGAT* and the Gln-dependent Asn-producing gene *AS* had relatively minor functional effects during early larval stages compared to *GDH* and *GOT1* but became increasingly significant during silk production (Figure 1; Supplementary Figure S3B). *GS*, *GOGAT*, and *AS* exhibited lower expression in early instar larvae (Figure 1A), and their disruption resulted in milder effects on body weight compared to *GDH* and *GOT1* in these stages (Figure 2B). This suggests that the re-assimilation of ammonia for Gln synthesis, which is subsequently converted to Glu and Asn, is more crucial for silk production. During the early instar stages, nitrogen demand is relatively low, and the nitrogen-rich diet provided by young mulberry leaves is sufficient to meet metabolic requirements. Both GDH and GOT1 utilize Glu as a substrate, exhibiting a competitive and partially redundant functional relationship. In quiescent mammalian cells, GDH primarily directs Glu-derived carbon metabolism, while proliferating cells catabolize more Glu via transaminases, such as GOT1, linking non-essential amino acid synthesis to α-KG generation and TCA cycle anaplerosis (Coloff et al., 2016). A similar dynamic may exist in *B. mori*, where *GDH* and *GOT1* play dominant roles in growth during the first to third instars, while *GS*, *GOGAT*, and *AS* become more essential in later developmental stages, particularly for silk synthesis. *GDH* appears to be functionally significant throughout multiple stages of silkworm development and metamorphosis, whereas *GOT1* may be more important during early larval development rather than in silk production. Consequently, artificial selection on *GDH* and *GOT1* may contribute more to silkworm larval growth than to silk spinning.

Rapid growth and developmental expansion of both the whole body and silk glands began in the middle of the fifth instar (Ma et al., 2024) and peaked at its conclusion (Figure 3C). During this period, nitrogen assimilation intensified, driven by increased dietary intake and enhanced ammonia re-assimilation. *GS*, *GOGAT*, and *AS* were consistently up-regulated throughout this phase (Figure 1A), and their disruption significantly impacted silk protein genes (Figure 3D). As the primary enzyme responsible for ammonia re-assimilation, GS was shown to exert the most significant contribution to silk yield (Figure 3A). Despite its low expression in silk glands (Figure 3C), its product, Gln, can penetrate the cell membrane of silk gland cells, serving as both a nitrogen source and an energy substrate for silk gland metabolism. Our previous study suggested that *GS* evolved convergently in both silkworms and crop plants (Xiang et al., 2018). In crops, urease activity —either from soil-derived enzymes or endogenous plant urease —catalyzes the breakdown of urea into ammonium (NH_4^+), which is then assimilated by GS as a nitrogen source. A similar mechanism has been proposed in silkworms, where dietary urease from mulberry leaves facilitates the conversion of urea to NH_4^+ (Hirayama et al., 1999), which is then incorporated into nitrogen metabolism via GS. Notably, dietary urea supplementation has been shown to increase silk gene expression and silk yield (Zhu et al., 2015). Based on these findings, we propose that *GS* functions convergently in both domestic plants and insects, contributing to efficient nitrogen utilization for agriculturally and economically important traits. Unlike *GS*, *GOGAT* and *AS* functioned directly within the silk glands, as evidenced by their higher expression levels in this tissue (Figure 1B; Supplementary Figure S1). Notably, *AS* appeared to have a greater contribution to silk production than *GOGAT*, given its higher expression in silk glands (Figure 1B; Supplementary Figure S3B), and the more severe reduction in cocoon thickness following *AS* disruption The GS/GOGAT cycle has been proposed as a key ammonia re-assimilation system in silk-spinning moths (Hirayama & Nakamura, 2002). However, its functional contributions to silk gland biology appear to be distinct. As mentioned above, GS plays a pivotal role in ammonia assimilation in *B. mori*, and previous studies have demonstrated that inhibition of *GS* using methionine sulfoximine results in a rapid and substantial accumulation of ammonia in the hemolymph (Hirayama et al., 1997). Disruption of *GS* likely led to an increase in hemolymph ammonia concentration, which may have contributed to cellular stress and potential damage, particularly in the posterior silk gland (PSG) (Figure 3C). Ammonia detoxification, catalyzed by GDH, is essential for maintaining metabolic balance (Hirayama et al., 1997). Additionally, *GS* disruption not only impairs ammonia assimilation but also deprives cells of a critical nitrogen source, creating a metabolic state akin to amino acid starvation, which has been shown to induce *AS* expression (Chen et al., 2004). Consistent with this, we detected elevated mRNA levels of *AS* and *GDH* following *GS* disruption. However, only GDH exhibited increased enzymatic activity, whereas AS remained unchanged. This discrepancy contrasts with the response observed in *GOGAT* mutants and may partially explain why *GS* mutants did not develop enlarged silk glands at the end of the final larval instar.

GOGAT has been identified exclusively in insects (Hirayama et al., 1998), suggesting its evolutionary specialization in nitrogen utilization among silk-producing species. Notably, *GOGAT* disruption resulted in a dramatic expansion of the silk glands, a phenotype that contrasts sharply with the role of its plant ortholog, *NADH-GOGAT*, in nitrogen metabolism (Yamaya & Kusano, 2014). This abnormal glandular overgrowth was likely driven by the pronounced activation of *AS* and *GDH* in response to *GOGAT* disruption. Knockout of *GOGAT* led to an accumulation of both Gln and α-KG, two highly dynamic prototrophic supporters with rapid turnover (Kodama et al., 2020). Consistent with this metabolic shift, our results showed an increase in the enzymatic activities of AS and GDH, suggesting a compensatory response to altered nitrogen flux. We hypothesize that this metabolic crosstalk extends across the silk-spinning transition. *AS* is well-characterized in tumor biology, where it supports rapid cell proliferation and suppresses apoptosis (Fontes et al., 2024; Knott et al., 2018; Krall et al., 2016; Li et al., 2016; Yuan et al., 2024; Zhang et al., 2016). Similarly, GDH primarily governs Glu-derived carbon metabolism in quiescent mammalian cells (Coloff et al., 2016) but can facilitate amino acid biosynthesis under ammonia-rich conditions, such as within the tumor

microenvironment (Spinelli et al., 2017). Similarly, *GOGAT* knockout in *B. mori* induced a degree of ammonia accumulation, and silk glands at the final instar stage exhibited phenotypic features reminiscent of tumor-like tissue. These findings suggest that prior to silk spinning, elevation of AS and GDH activity likely promotes non-essential amino acid synthesis, fueling excessive silk gland growth. From this perspective, *GOGAT* appears to play a unique role in precisely coordinating Gln and α-KG allocation within the silk glands, integrating nitrogen and carbon metabolism balance to ensure optimal silk protein synthesis. This coordination ensures the synthesis of silk proteins for cocoon production, a characteristic of metamorphosis, while preventing excessive glandular growth, a trait of the larval stage. Supporting this hypothesis, *GOGAT* expression in silk glands is modulated by reduced juvenile hormone levels (Hirayama & Nakamura, 2002). Collectively, these findings suggest that *GOGAT* functions as a metabolic coordinator, working in concert with *AS* and *GDH* to maintain nitrogen homeostasis and orchestrate silk gland development during metamorphosis.

Both *GS* and *GOGAT* mutants exhibited aberrant up-regulation of ribosome biogenesis in the silk glands of metamorphosis-arrested prepupae (Figure 4D). In contrast, ribosome biogenesis was significantly down-regulated in the silk glands of normal prepupae undergoing programmed cell death (Supplementary Figure S3C, D). This persistent translational activity may contribute to the maintenance of a larval-like state in the silk glands of metamorphosis-arrested mutants. In *GS* mutants, elevated ribosomal activity was associated with the up-regulation of the Hippo signaling pathway and several other pathways involved in organ size regulation (Figure 7C). Notably, the observed up-regulation of the *Expanded* (*Ex*) gene, a key regulator of the Hippo signaling pathway (Su et al., 2017), suggests that silk glands at the end of the final larval instar underwent organ size modulation. In *GOGAT* mutants, excessive translational activity appeared to support another hyperactive RNA-processing mechanism—the spliceosome. These highly active cellular machineries likely reflect an abundant amino acid pool. The up-regulation of *AS* and *GDH* in these mutants may contribute to nitrogen accumulation, potentially leading to metabolic eutrophication, which, in turn, could interfere with programmed cell death of silk gland cells in *ΔGOGAT*. This hypothesis warrants further investigation.

The functional role and molecular mechanisms of *AS* in silk gland biology during metamorphosis differ fundamentally from those of the two ammonia assimilation-related genes. AS catalyzes the *de novo* synthesis of Asn from Gln, playing a pivotal role in protein and nucleotide biosynthesis (Krall et al., 2016). While AS and GOGAT compete for Gln, their functions in silk glands are distinct. *AS* is particularly crucial during the late larval stage, supporting silk gland development. Our results showed that *AS* disruption in the silk glands led to a marked increase in both *GOT* mRNA expression and enzymatic activity (Figure 6), indicating a direct functional coupling between *AS* and *GOGAT* during larva-pupa metamorphosis. This metabolic up-regulation sharply contrasted with the down-regulation of metabolic pathways observed in the degrading silk glands of normal prepupae (Supplementary Figure S3C, D), further supporting the notion that *ΔAS* silk glands remained in an active state rather than undergoing programmed degeneration (Figure 4C, D). Additionally, *AS* disruption severely impaired the Hippo signaling pathway, particularly affecting the expression of *yki* (Supplementary Figure S4B), a key downstream effector essential for programmed cell death in silk glands and silkworm metamorphosis. Its dysregulation in the absence of *AS* strongly hinders this process (Xu et al., 2018). Based on these findings, we propose a novel regulatory role for *AS* in coordinating silk gland development and subsequent programmed cell death, potentially through an unidentified mechanism linking *AS* function to *yki*-mediated Hippo signaling.

Cocoon-spinning is a highly orchestrated process that facilitates the excretion of nitrogenous metabolites from systemic metabolism and is strongly influenced by various factors, particularly nutritional status (Chen et al., 2022). While the developmental restrictions associated with nitrogen mobilization gene mutations may contribute to the observed changes in silk gland biology, this effect may differ in loss-of-function mutants of different genes. As discussed earlier, the silk gland phenotype in *GOT1* mutants was likely a secondary consequence of impaired larval development. In contrast, *GOGAT*, *AS*, and *GS* mutants exhibited distinct and direct phenotypic alterations in the silk glands. Specifically, *GOGAT* mutants developed abnormally enlarged silk glands, while *AS* mutants displayed delayed programmed cell death. These findings suggest that *GS*, *GOGAT*, and *AS* play direct roles in regulating silk gland biology. Future studies employing silk gland-specific knockouts of these genes will be critical for further elucidating their precise functions.

This study provides new insights into both the consistent and gene-specific roles of nitrogen mobilization-related genes in silk production, silk gland biology, and the broader developmental processes governing *B. mori* metamorphosis. We identified significant metabolic crosstalk among these genes and uncovered a previously unrecognized link between nutritional regulation and metamorphosis. Artificial selection on nitrogen metabolism-related genes has enabled the domesticated silkworm to efficiently coordinate nitrogen utilization across developmental stages, facilitating its adaptation to the substantially increased dietary intake required for silk protein synthesis.

DATA AVAILABILITY

Transcript sequencing data were deposited in the Genome Sequence Archive (GSA) database (CRA021436), Science Data Bank (doi: 10.57760/sciencedb.j00139.00152), and NCBI Sequence Read Archive (SRA) (BioProjectID SAMN38861458–SAMN39961493 and SAMN38861269–SAMN38861280).

SUPPLEMENTARY DATA

Supplementary data to this article can be found online.

COMPETING INTERESTS

The authors declare that they have no competing interests.

AUTHORS' CONTRIBUTIONS

M.Y.Y. and H.X. designed the research; M.Y.Y. and X.Y. performed the research; H.X. and Y.P.H. contributed reagents and analytic tools; M.Y.Y., X.Y., J.W.C., J.H.X., L.J.X., L.S.Q., D.B.C., X.L.T., Z.L.L., Y.P.H., and H.X. analyzed the data; M.Y.Y. and H.X. draft the manuscript; M.Y.Y., M.W., X.L.T., and H.X. revised the manuscript. All authors read and approved the final version of the manuscript.

ACKNOWLEDGMENTS

We thank Prof. Shuai Zhan (Key Laboratory of Insect Developmental and

Evolutionary Biology, Center for Excellence in Molecular Plant Sciences, Shanghai Institute of Plant Physiology and Ecology, Chinese Academy of Sciences) and Sheng Li (Guangdong Provincial Key Laboratory of Insect Developmental Biology and Applied Technology, Institute of Insect Science and Technology, School of Life Sciences, South China Normal University) for their insightful comments. We thank Yan Wu and Li-Zhi Wang (Guangdong Provincial Key Laboratory of Insect Developmental Biology and Applied Technology, Institute of Insect Science and Technology, School of Life Sciences, South China Normal University) for their help in handling the experiments.

REFERENCES

Chen H, Pan YX, Dudenhausen EE, et al. 2004. Amino acid deprivation induces the transcription rate of the human asparagine synthetase gene through a timed program of expression and promoter binding of nutrient-responsive basic region/leucine zipper transcription factors as well as localized histone acetylation. *Journal of Biological Chemistry*, **279**(49): 50829–50839.

Chen XD, Ye AH, Wu XH, et al. 2022. Combined analysis of silk synthesis and hemolymph amino acid metabolism reveal key roles for glycine in increasing silkworm silk yields. *International Journal of Biological Macromolecules*, **209**(Pt B): 1760–1770.

Coloff JL, Murphy JP, Braun CR, et al. 2016. Differential glutamate metabolism in proliferating and quiescent mammary epithelial cells. *Cell Metabolism*, **23**(5): 867–880.

Cui Y, Zhu YN, Lin YJ, et al. 2018. New insight into the mechanism underlying the silk gland biological process by knocking out fibroin heavy chain in the silkworm. *BMC Genomics*, **19**(1): 215.

Daimon T, Hirayama C, Kanai M, et al. 2010. The silkworm *Green b* locus encodes a quercetin 5-*O*-glucosyltransferase that produces green cocoons with UV-shielding properties. *Proceedings of the National Academy of Sciences of the United States of America*, **107**(25): 11471–11476.

Fontes MG, Silva C, Roldán WH, et al. 2024. Exploring the potential of asparagine restriction in solid cancer treatment: recent discoveries, therapeutic implications, and challenges. *Medical Oncology*, **41**(7): 176.

Goncu E, Parlak O. 2008. Some autophagic and apoptotic features of programmed cell death in the anterior silk glands of the silkworm, *Bombyx mori*. *Autophagy*, **4**(8): 1069–1072.

Hirayama C, Konno K, Shinbo H. 1996. Utilization of ammonia as a nitrogen source in the silkworm, *Bombyx mori*. *Journal of Insect Physiology*, **42**(10): 983–988.

Hirayama C, Konno K, Shinbo H. 1997. The pathway of ammonia assimilation in the silkworm, *Bombyx mori*. *Journal of Insect Physiology*, **43**(10): 959–964.

Hirayama C, Saito H, Konno K, et al. 1998. Purification and characterization of NADH-dependent glutamate synthase from the silkworm fat body (*Bombyx mori*). *Insect Biochemistry and Molecular Biology*, **28**(7): 473–482.

Hirayama C, Sugimura M, Shinbo H. 1999. Recycling of urea associated with the host plant urease in the silkworm larvae, *Bombyx mori*. *Journal of Insect Physiology*, **45**(1): 15–20.

Hirayama C, Nakamura M. 2002. Regulation of glutamine metabolism during the development of *Bombyx mori* larvae. *Biochimica et Biophysica Acta (BBA) - General Subjects*, **1571**(2): 131–137.

Horie Y, Watanabe K. 1986. Daily utilization of nitrogen in food by the silkworm, *Bombyx mori* (Lepidoptera: Bombycidae). *Applied Entomology and Zoology*, **21**(2): 289–298.

Kawamoto K, Kawamoto T, Shiba H, et al. 2014. A histochemical study of the posterior silk glands of *Bombyx mori* during metamorphosis from larvae to pupae using frozen sections. *Biotechnic & Histochemistry*, **89**(2): 145–152.

Knott SRV, Wagenblast E, Khan S, et al. 2018. Asparagine bioavailability governs metastasis in a model of breast cancer. *Nature*, **554**(7692): 378–381.

Kodama M, Oshikawa K, Shimizu H, et al. 2020. A shift in glutamine nitrogen metabolism contributes to the malignant progression of cancer. *Nature Communications*, **11**(1): 1320.

Krall AS, Xu SL, Graeber TG, et al. 2016. Asparagine promotes cancer cell proliferation through use as an amino acid exchange factor. *Nature Communications*, **7**: 11457.

Langfelder P, Horvath S. 2008. WGCNA: an R package for weighted correlation network analysis. *BMC Bioinformatics*, **9**: 559.

Li H, Zhou FS, Du WH, et al. 2016. Knockdown of asparagine synthetase by RNAi suppresses cell growth in human melanoma cells and epidermoid carcinoma cells. *Biotechnology and Applied Bioche* gene expression in the silk gland of the silkworm (*Bombyx mori*) during metamorphosis. *Canadian Journal of Zoology*, **88**(12): 1169–1178.

Lőrincz P, Juhász G. 2020. Autophagosome-lysosome fusion. *Journal of Molecular Biology*, **432**(8): 2462–2482.

Love MI, Huber W, Anders S. 2014. Moderated estimation of fold change and dispersion for RNA-seq data with DESeq2. *Genome Biology*, **15**(12): 550.

Ma Y, Li QJ, Tang YY, et al. 2024. The architecture of silk-secreting organs during the final larval stage of silkworms revealed by single-nucleus and spatial transcriptomics. *Cell Reports*, **43**(7): 114460.

Melo-Oliveira R, Oliveira IC, Coruzzi GM. 1996. Arabidopsis mutant analysis and gene regulation define a nonredundant role for glutamate dehydrogenase in nitrogen assimilation. *Proceedings of the National Academy of Sciences of the United States of America*, **93**(10): 4718–4723.

Montali A, Romanelli D, Cappellozza S, et al. 2017. Timing of autophagy and apoptosis during posterior silk gland degeneration in *Bombyx mori*. *Arthropod Structure & Development*, **46**(4): 518–528.

Patro R, Duggal G, Love MI, et al. 2017. Salmon provides fast and bias-aware quantification of transcript expression. *Nature Methods*, **14**(4): 417–419.

Shannon P, Markiel A, Ozier O, et al. 2003. Cytoscape: a software environment for integrated models of biomolecular interaction networks. *Genome Research*, **13**(11): 2498–2504.

Soneson C, Love MI, Robinson MD. 2015. Differential analyses for RNA-seq: transcript-level estimates improve gene-level inferences. *F1000Research*, **4**: 1521.

Spinelli JB, Yoon H, Ringel AE, et al. 2017. Metabolic recycling of ammonia via glutamate dehydrogenase supports breast cancer biomass. *Science*, **358**(6365): 941–946.

Su T, Ludwig MZ, Xu JJ, et al. 2017. Kibra and Merlin activate the Hippo pathway spatially distinct from and independent of Expanded. *Developmental Cell*, **40**(5): 478–490. e3.

Tan AJ, Fu GL, Jin L, et al. 2013. Transgene-based, female-specific lethality system for genetic sexing of the silkworm, *Bombyx mori*. *Proceedings of the National Academy of Sciences of the United States of America*, **110**(17): 6766–6770.

Tong XL, Han MJ, Lu KP, et al. 2022. High-resolution silkworm pan-genome provides genetic insights into artificial selection and ecological adaptation. *Nature Communications*, **13**(1): 5619.

Wang H, Wang YL, Wu CJ, et al. 2016. Changes in 30K protein synthesis during delayed degeneration of the silk gland by a caspase-dependent pathway in a *Bombyx* (silkworm) mutant. *Journal of Comparative Physiology B*, **186**(6): 689–700.

Xia QY, Guo YR, Zhang Z, et al. 2009. Complete resequencing of 40 genomes reveals domestication events and genes in silkworm (*Bombyx*). *Science*, **326**(5951): 433–436.

Xia QY, Li S, Feng QL. 2014. Advances in silkworm studies accelerated by the genome sequencing of *Bombyx mori*. *Annual Review of Entomology*,

59: 513–536.
Xiang H, Liu XJ, Li MW, et al. 2018. The evolutionary road from wild moth to domestic silkworm. *Nature Ecology & Evolution*, **2**(8): 1268–1279.
Xu J, Chen SQ, Zeng BS, et al. 2017. *Bombyx mori* P-element somatic inhibitor (BmPSI) is a key auxiliary factor for silkworm male sex determination. *PLoS Genetics*, **13**(1): e1006576.
Xu J, Chen RM, Chen SQ, et al. 2019. Identification of a germline-expression promoter for genome editing in *Bombyx mori*. *Insect Science*, **26**(6): 991–999.
Xu X, Zhang Z, Yang Y, et al. 2018. Genome editing reveals the function of Yorkie during the embryonic and early larval development in silkworm, *Bombyx mori*. *Insect Molecular Biology*, **27**(6): 675–685.
Yamaya T, Kusano M. 2014. Evidence supporting distinct functions of three cytosolic glutamine synthetases and two NADH-glutamate synthases in rice. *Journal of Experimental Botany*, **65**(19): 5519–5525.
Ye XG, Tang XL, Zhao S, et al. 2021. Mechanism of the growth and development of the posterior silk gland and silk secretion revealed by mutation of the *fibroin light chain* in silkworm. *International Journal of Biological Macromolecules*, **188**: 375–384.
Yuan Q, Yin LY, He J, et al. 2024. Metabolism of asparagine in the physiological state and cancer. *Cell Communication and Signaling*, **22**(1): 163.
Zhang BY, Fan JJ, Zhang XY, et al. 2016. Targeting asparagine and autophagy for pulmonary adenocarcinoma therapy. *Applied Microbiology and Biotechnology*, **100**(21): 9145–9161.
Zhu QY, Li MJ, Chen YB, et al. 2015. Effects of different nitrogen-containing nutrients on silk production and expression of silk fibroin heavy chain gene. *Science of Sericulture*, **41**(4): 658–662. (in Chinese)